Biochemical characterization of the interaction between KRAS and Argonaute 2

Jessica J. Waninger [a,b,c,i], Tyler S. Beyett [d], Varun V. Gadkari [e], Ronald F. Siebenaler [b,i], Carson Kenum [a], Sunita Shankar [a,f,i], Brandon T. Ruotolo [e], Arul M. Chinnaiyan [a,f,g,h,i], John J. G. Tesmer [j,*]

[a] Michigan Center for Translational Pathology, University of Michigan, Ann Arbor, MI, 48109, USA
[b] Department of Medical Education, University of Michigan, Ann Arbor, MI, USA
[c] Department of Cellular and Molecular Biology, University of Michigan, Ann Arbor, MI, USA
[d] Life Sciences Institute, University of Michigan, Ann Arbor, MI, USA
[e] Department of Chemistry, University of Michigan, Ann Arbor, MI, USA
[f] Department of Pathology, University of Michigan, Ann Arbor, MI, USA
[g] Howard Hughes Medical Institute, University of Michigan, Ann Arbor, MI, USA
[h] Department of Urology, University of Michigan, Ann Arbor, MI, USA
[i] Rogel Cancer Center, University of Michigan, Ann Arbor, MI, USA
[j] Departments of Biological Sciences and Medicinal Chemistry & Molecular Pharmacology, Purdue University, Indiana, USA

A B S T R A C T

Oncogenic mutations in KRAS result in a constitutively active, GTP-bound form that in turn activates many proliferative pathways. However, because of its compact and simple architecture, directly targeting KRAS with small molecule drugs has been challenging. Another approach is to identify targetable proteins that interact with KRAS. Argonaute 2 (AGO2) was recently identified as a protein that facilitates RAS-driven oncogenesis. Whereas previous studies described the *in vivo* effect of AGO2 on cancer progression in cells harboring mutated KRAS, here we sought to examine their direct interaction using purified proteins. We show that full length AGO2 co-immunoprecipitates with KRAS using purified components, however, a complex between FL AGO2 and KRAS could not be isolated. We also generated a smaller N-terminal fragment of AGO2 (NtAGO2) which is believed to represent the primary binding site of KRAS. A complex with NtAGO2 could be detected via ion-mobility mass spectrometry and size exclusion chromatography. However, the data suggest that the interaction of KRAS with purified AGO2 (NtAGO2 or FL AGO2) is weak and likely requires additional cellular components or proteo-forms of AGO2 that are not readily available in our purified assay systems. Future studies are needed to determine what conformation or modifications of AGO2 are necessary to enrich KRAS association and regulate its activities.

1. Introduction

Mutations in the *RAS* gene family account for a large percentage of all known genetic aberrations in cancer. Of the three RAS homologues, KRAS is the most frequently mutated, driving the three most lethal cancer types in the United States: pancreatic ductal adenocarcinoma (PDAC), colorectal cancer, and lung adenocarcinoma [1,2]. Given its importance in cancer pathogenesis, there have been intense efforts to understand the RAS signaling network and the molecular basis underlying its function. KRAS is a small GTPase that relays mitogenic signals from growth factor receptors at the membrane to the nucleus when bound to GTP [3,4]. Under physiological conditions, nucleotide cycling

on KRAS is accelerated and regulated by guanine exchange factors (GEFs) and GTPase activating proteins (GAPs), which promote GTP loading and hydrolysis, respectively [5]. The KRAS structure is compact, comprised only of a G-domain (residues 1–166) and a hypervariable C-terminal region (residues 167–188) that is important for membrane association. Within the G-domain are three elements important for KRAS function: the phosphate-binding loop (P-loop) and switch I and II. The P-loop is essential for nucleotide coordination, whereas the switches adopt different conformations depending on the nucleotide bound and serve as the primary binding interface for KRAS effector targets and regulators. Downstream effector proteins such as RAF or PI3K use the switch regions for association and only recognize their GTP-bound,

active conformation [6,7]. Once active, KRAS initiates a cascade of signaling events that promote pro-cancer phenotypes, including proliferation, survival, and metastasis. The P-loop is the site of two prominent KRAS driver mutations, which occur at the 12th and 13th codon, respectively [8,9]. Along with mutations at the 61st codon, perturbation of these sites interferes with the intrinsic GTPase activity of KRAS and prohibits the binding of GAPs, leaving KRAS in an active state. Despite a clear justification in pursing KRAS as a target and decades of dedicated investigation, therapeutic intervention for most KRAS-driven cancers remains a challenge. Even the most recent therapeutics targeting G12C KRAS in non-small cell lung cancer (NSCLC) are becoming ineffective due to the development of drug resistance [10].

Protein–protein interactions are critical in many oncogenic processes and can potentially be exploited in therapeutic development. Recently, Argonaute 2 (AGO2), the catalytic component of the RNA-induced silencing complex (RISC), was reported to be a novel interactor of RAS [11]. AGO2 is a large and dynamic protein with four distinct domains connected through linker regions [12]. It performs the final step in miRNA maturation, associates with other proteins to form the RISC complex, and cleaves the miRNA:mRNA duplex [13]. These functions are regulated in a context-specific way through a variety of post-translational modifications [14]. Although AGO2 is independently associated with oncogenesis [15], it was demonstrated that AGO2 expression was necessary for oncogenic transformation in mutant
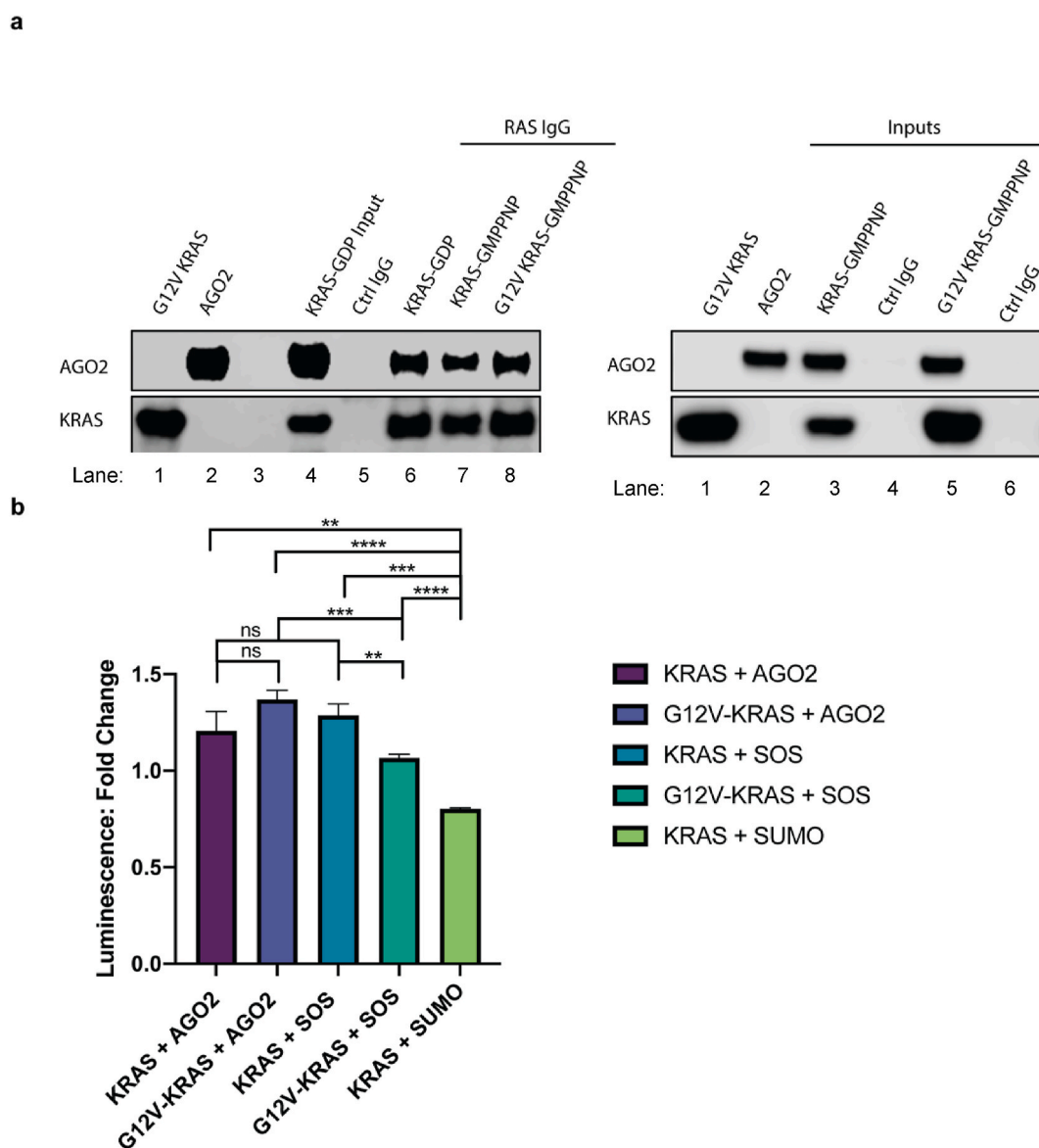

Fig. 1. Full-length AGO2 associates with KRAS and G12V-KRAS regardless of nucleotide status. **a)** Purified KRAS·GDP, KRAS·GMPPNP, or G12V KRAS·GMPPNP were each mixed with purified FL AGO2. RAS10 IgG was added to the purified protein samples and incubated overnight. Immune complexes were precipitated using magnetic beads and the samples were probed for KRAS and AGO2 using western blot analysis. Left panel, lane 1: purified G12V KRAS; lane 2: purified FL AGO2; lane 3: empty lane; lane 4: input containing KRAS·GDP and FL AGO2; lane 5: IP of KRAS·GDP–FL AGO2 sample using a control, non-specific mouse IgG; lanes 6–8: IP of KRAS·GDP–Fl AGO2 (6), KRAS·GMPPNP–FL AGO2 (7), or G12V-KRAS·GMPPNP–FL AGO2 (8) using a RAS specific IgG. Right panel, lane 1: purified G12V KRAS; lane 2: purified FL AGO2; lanes 3–4: the total protein input to the KRAS·GMPPNP–FL AGO2 sample (3) and IP using a control, non-specific mouse IgG (4); lanes 5–6: the total protein input to the G12V-KRAS·GMPPNP–FL AGO2 sample (5) and IP using a control, non-specific mouse IgG (6). **b)** Lumit ImmunoAssay of KRAS·GTP or G12V-KRAS·GTP complexed with either full length AGO2, SOS or SUMO protease. Student's T-test was used to compare mean luminescence fold change between each sample following RAS10 antibody background signal subtraction. Mean luminescence values were measured from three independent experiments performed in triplicate. Error bars represent the standard deviation of the mean luminescence for each sample. Full length western blot images can be found in Supplementary Fig. S3. **, $0.001 < P < 0.01$; ***, $0.0001 < P < 0.001$; ****p < 0.0001; ns, not significant.

KRAS-dependent cell lines [11]. More recently, these findings were expanded in a genetically engineered mouse model of pancreatic ductal adenocarcinoma (PDAC). AGO2 was required for the transition from pancreatic intraepithelial lesions (PanIN) to PDAC, and loss of AGO2 resulted in oncogene induced senescence via KRAS hyperactivation. Furthermore, the interaction between AGO2 and wild-type KRAS was disrupted following the phosphorylation of AGO2 by the epidermal growth factor receptor (EGFR), allowing KRAS association with activating GEFs such as SOS [16].

Although there is cellular and *in vivo* evidence for association of KRAS with AGO2, many molecular details of their interaction remain unclear. We investigated formation of their complex using purified proteins via a series of biophysical and biochemical techniques with the ultimate goal of structural characterization. In previous work, mutagenesis experiments suggested that AGO2 uses its N-domain to associate with the switch II region of KRAS [11]. The N-domain serves as a wedge between the guide and passenger strand to facilitate unwinding in the RISC complex, and is therefore important in miRNA maturation [17]. Given the complexity and conformational heterogeneity of full-length AGO2 (FL AGO2), we focused primarily on N-terminal fragments of AGO2. Although we confirmed a direct interaction, it was low affinity and transient, suggesting that other factors help to stabilize the KRAS-AGO2 complex in cells.

2. Results

2.1. Full-length AGO2 associates with soluble and G12V-KRAS regardless of its nucleotide-bound state

To confirm that AGO2 directly associates with KRAS, we purified FL AGO2, and tested the association of a soluble variant of KRAS (residues 1–166, hereafter referred to simply as KRAS), and its constitutively active mutant G12V-KRAS in various nucleotide states via co-IP experiments followed by western blot analysis. Consistent with IPs from cellular lysates published in prior studies, there was equivalent pulldown of FL AGO2 following RAS-IP irrespective of mutation or nucleotide status (Fig. 1a) [11]. Images for the full-length western blots can be found in Supplementary Fig. S1. We also used a proximity-based, antibody-mediated luminescence assay to confirm the association of AGO2 to both KRAS constructs. In these experiments either KRAS·GTP or G12V-KRAS·GTP was added at equimolar ratios to purified FL AGO2, SOS (a GEF for KRAS), or SUMO protease (as a non-specific protein control). The fold-change of luminescent signal for both KRAS–FL AGO2 constructs and KRAS-SOS was significantly increased compared to the negative control SUMO (Fig. 1b). As expected, there was no difference between KRAS and G12V-KRAS–AGO2 association, suggesting that their association is nucleotide independent under these experimental conditions. There was, however, a significant difference between KRAS–SOS and G12V-KRAS–SOS association, which is to be expected given that SOS primarily associates with GDP-bound or apo forms of RAS [18].

2.2. Direct interaction of NtAGO2 with KRAS can be detected by SEC and MALS

Using the same constructs as above, we sought to isolate a complex between purified FL AGO2 and both KRAS constructs via analytical size exclusion chromatography (SEC). This, however, failed to show a protein complex (Supplementary Fig. S2), suggesting that only a minute fraction of the FL AGO2 expressed from our eukaryotic system is in a form compatible with KRAS association. This would explain why a complex is detectable via the more sensitive antibody-mediated techniques demonstrated above and lost in a less sensitive experimental setting.

In prior cell-based mutagenesis experiments the interaction between AGO2 and KRAS was shown to involve the switch II region of KRAS and the N-domain of AGO2 [11]. These results however do not necessarily

indicate a direct interaction exclusive to these elements. Given the heterogeneity of post-translational modifications, miRNA status, and the influence of other interaction partners of AGO2 in eukaryotic cells, we expressed and purified residues 55–137 of its N-domain (NtAGO2) in *E. coli*. Validation of the interaction using this fragment was prioritized because it would also facilitate future X-ray crystallographic analysis. We first tested complex formation with G12V-KRAS·GMPPNP via SEC. The G12V-KRAS–NtAGO2 complex eluted at an earlier volume compared to either individual protein (Fig. 2a) (see Supplementary Fig. S3 for full SDS-PAGE gel). Re-evaluation of the pooled complex fractions by SEC resulted in a rightward shift and disappearance of the NtAGO2 fragment, suggesting that the complex is transient and that NtAGO2 alone is unstable and aggregated between runs. To determine the molecular weight (MW) of the complex eluting from the size exclusion column, multi-angle light scattering (MALS) data was collected. These data revealed that the MW of the first peak eluted was 25 ± 1.5 kDa, consistent with a 1:1 complex between NtAGO2 ($\sim$10 kDa) and G12V KRAS·GTP ($\sim$18 kDa). Approximately 10% of the total protein was in complex, whereas the remaining monomeric proteins eluted at their expected monomeric MW values (Fig. 2b). These data confirm that purified NtAGO2 directly binds to KRAS but that their interaction is likely transient.

2.3. Analysis of the NtAGO2–KRAS complex by ion mobility-mass spectrometry (IM-MS)

Next, native IM-MS was employed to further validate the transient interaction between NtAGO2 and G12V-KRAS. This technique combines ion mobility spectrometry, a gas phase separation analogous to electrophoreses, with highly sensitive mass spectrometry detection. Using gentle sample preparation and ionization practices, it is possible to preserve solution-phase protein structures [19,20] and non-covalent interactions of varying affinities [21–23]. Upon IM-MS analysis of a 2:1 mixture of NtAGO2 incubated with G12V-KRAS·GMPPNP, signals corresponding to NtAGO2 (9992.7 ± 0.4 Da), and G12V-KRAS·GMPPNP ($19,619 \pm 3$ Da) and the G12V-KRAS–NtAGO2 complex (MW: $29,710 \pm 20$ Da) were detected (Fig. 3A). Quantitation of signal intensities indicated that only $\sim$2.6 $\pm$ 0.7% NtAGO2 was in complex with G12V-KRAS, consistent with low affinity. Orientationally averaged collision cross sections ($^{DT}CCS_{He}$) were within the expected range for native globular proteins in this mass range [24] (Fig. 3B, Table S1). The 7^+ charge state of NtAGO2 is multimodal in the IM dimension, suggesting some conformational heterogeneity is present in the sample. In contrast, all charge states of KRAS are unimodal. The plasticity of NtAGO2 may also be a contributing factor to the bimodal IM distribution observed for the 12^+ charge state of the G12V-KRAS–NtAGO2 complex, which could be interpreted as G12V-KRAS interacting with more than one conformation of NtAGO2. To confirm the experimentally measured $^{DT}CCS_{He}$ values for the complex, crystal structures of G12V-KRAS (**PDB:4TQ9**) and a truncated structure of AGO2 (**PDB: 4W5N**) corresponding to NtAGO2 were computationally docked using pyDockWEB, a rigid-body protein-protein docking tool [25]. Theoretical CCS's ($^{T}CCS_{He}$) were computed for the resulting predicted complex structures (n = 100) using IMPACT projection approximation [26]. An excellent correlation exists between experimentally measured CCS, and IMPACT computed CCS from crystal structures, indicating that the gas phase protein ions retain their solution structure [27]. The distribution of $^{T}CCS_{He}$'s ($\sim$21–23 nm^2), is in good agreement with the experimentally measured $^{DT}CCS_{He}$'s (22–25 nm^2) further supporting that the signals observed in the IM-MS experiment correspond to a G12V-KRAS–NtAGO2 complex (Fig. 3C, Table S2).

2.4. Thermal stability of NtAGO2 in complex with KRAS

FL AGO2 co-IPs with KRAS irrespective of its mutation status or nucleotide state [11] (Fig. 1a), in contrast to all known RAS regulators and effectors, which are nucleotide selective. As such, we set out to
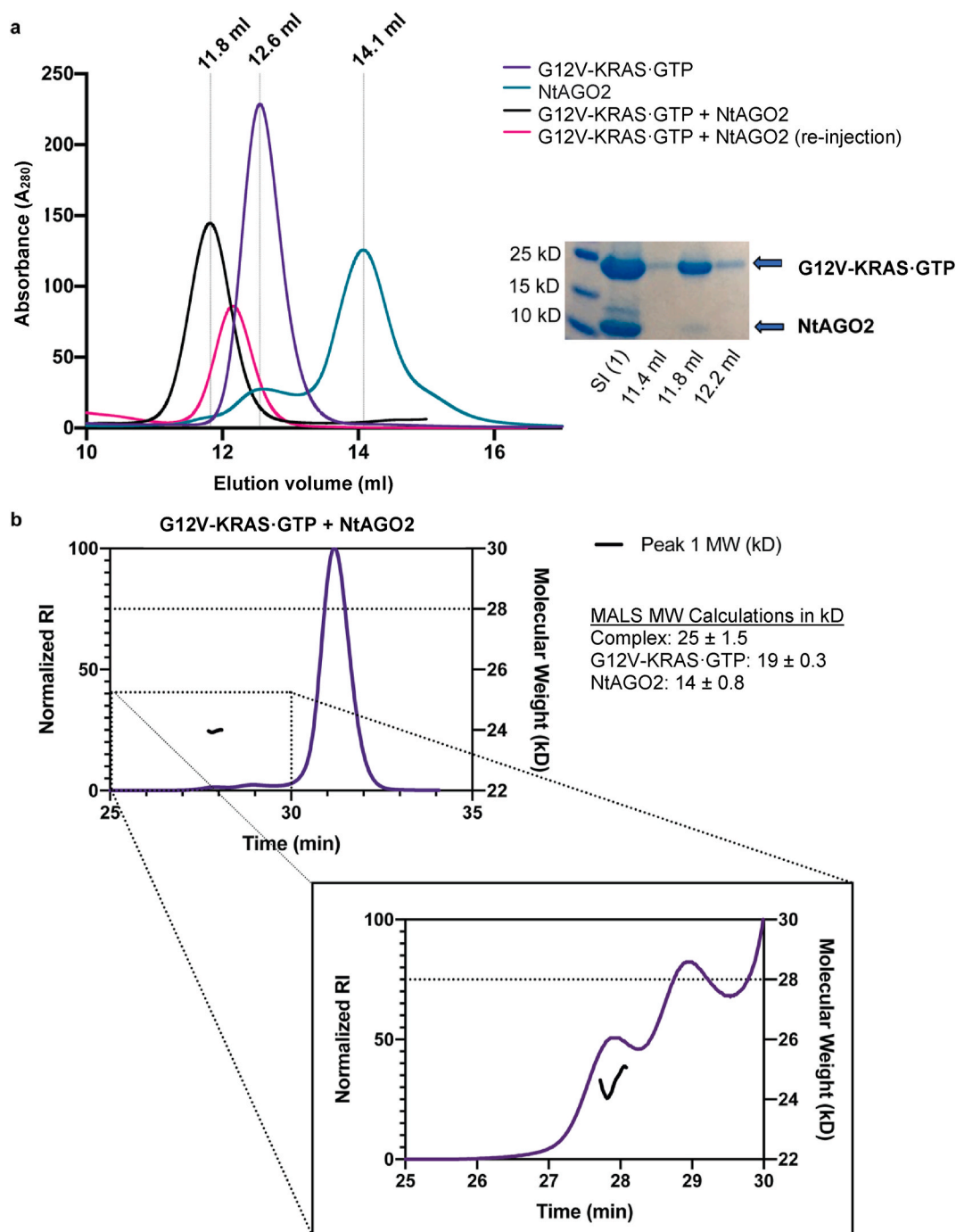
Fig. 2. A stoichiometric G12V-KRAS·GTP–NtAGO2 complex can be isolated via SEC. **a)** Raw A_{280} SEC trace of three separate runs: G12V-KRAS alone (purple), NtAGO2 alone (teal), and their complex (black). The pink curve represents the SEC tracing following the re-injection of the G12V-KRAS–NtAGO2 complex peak. SDS-PAGE gel (right) represents the sample injected (SI) and fractions at 11.4, 11.8, and 12.2 mL elution volumes of the G12V-KRAS–NtAGO2 complex (black). Full gel can be found in Supplementary Fig. S4. Vertical dotted lines represent the volume of the center of each peak. **b)** Normalized refractive index (RI) values for SEC-MALS trace (purple) of the G12V-KRAS–NtAGO2 complex. The black line represents the molecular weight calculation for the first peak. The bottom right panel is a trimmed and re-normalized version of the upper left panel. MALS MW calculations are tabulated. Representative tracings are shown. (For interpretation of the references to color in this figure legend, the reader is referred to the Web version of this article.)

evaluate both protein stability and nucleotide dependence of the interaction of NtAGO2 using differential scanning fluorimetry (DSF). Purified KRAS and G12V-KRAS were loaded with either GDP·Mg^{2+} or GTP·Mg^{2+} and added at equimolar ratios to purified NtAGO2. As expected, the addition of GDP or GTP to both KRAS constructs resulted in large positive shifts in melting point, indicating greater protein stability. Interestingly, the addition of NtAGO2 to nucleotide-bound KRAS (Fig. 4a), but not G12V-KRAS (Fig. 4b), appeared to cause protein unfolding or

aggregation as seen by the high background fluorescence intensity and the lack of a clear melting transition.

2.5. Affinity of NtAGO2 for KRAS

In attempts to determine interaction binding constants, biolayer interferometry (BLI) and isothermal titration calorimetry (ITC) were performed. BLI was done by immobilizing biotinylated G12V-KRAS and
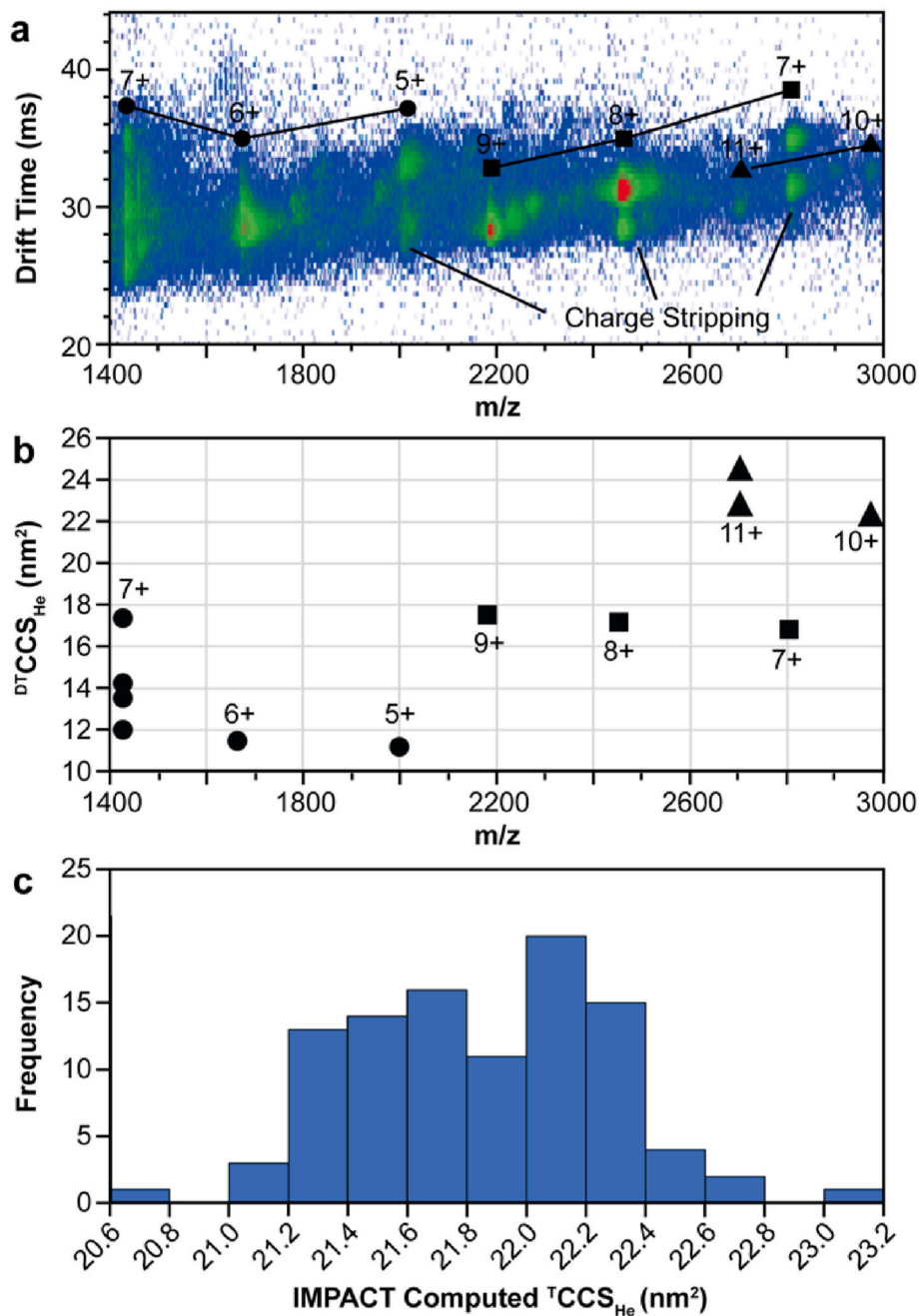
Fig. 3. Ion mobility-mass spectrometry (**IM-MS**) of G12V-KRAS·GMPPNP, NtAGO2, and their complex. **a)** IM mass of G12V-KRAS, AGO2, and G12V-KRAS–AGO2 separated by mass and mobility. The first three charge states (circles) correspond to NtAGO2, the second three charge states (squares) correspond to G12V KRAS·GMPPNP, and the final two charge states (triangles) correspond to the complex between NtAGO2 and G12V-KRAS·GMPPNP. **b)** Corresponding CCS values for the individual proteins and their complexes. **c)** IMPACT computed CCS values from the 100 highest scoring docked G12V-KRAS·GDP–NtAGO2 complex structures. Plain mass spectra for the IM-MS data are shown in Supplementary Fig. S5.

then adding increasing concentrations of NtAGO2. Using association data from multiple NtAGO2 concentrations, a K_D of 34 $\pm$ 40 μM was estimated (Fig. 5a). There is concentration-dependent association of NtAGO2, though its extent is variable between replicates. Furthermore, NtAGO2 does not disassociate in a normal equilibrium fashion (Fig. 5b). The results from ITC also show non-ideal behavior. Upon titration of G12V-KRAS·GMP-PNP into a well containing NtAGO2, we measured heat release that was attenuated in the Tyr64-KRAS variant (Fig. 5c). Importantly, this variant was shown in previous publications to prevent the association of KRAS to AGO2 [11]. The calculated K_D averaged from two independent experiments was 6.4 $\pm$ 7 μM. However, the heat measured never returns to baseline, even after buffer matching, suggesting that there may be some protein aggregation in the sample cell. Although protein behavior in these assays was not ideal, the binding

constants obtained were in the 6–35 μM range, consistent with a low affinity interaction.

2.6. NtAGO2 has no effect on intrinsic RAS-GTPase activity or SOS-mediated nucleotide exchange

It was previously shown that FL AGO2 interferes with the ability of SOS to associate with KRAS and catalyze nucleotide exchange [16]. To determine whether the NtAGO2 fragment could replicate this behavior, we performed analogous luminescence-based GTPase assays to measure the intrinsic GTPase activity of both KRAS constructs as well as GEF-associated nucleotide exchange in the presence and absence of SOS. As expected, SOS alone significantly facilitated nucleotide exchange in KRAS but not in G12V-KRAS. NtAGO2 did not appear to interfere with
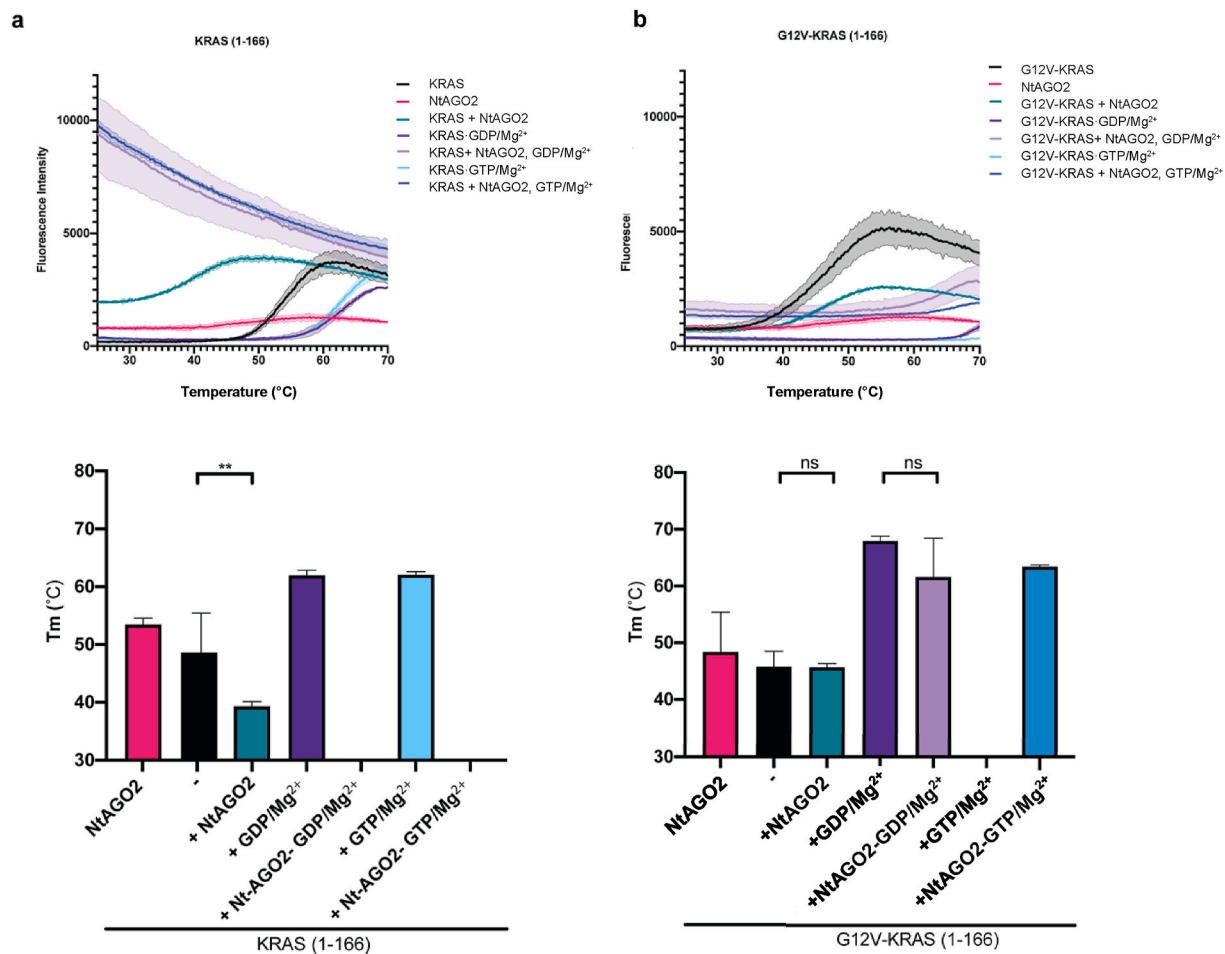
Fig. 4. DSF of KRAS variants (KRAS and G12V KRAS). **a)** Top panel: raw fluorescence intensity plotted against temperature for soluble KRAS with or without NtAGO2 in the apo, GDP, or GTP-loaded state. Bottom panel: melting temperature (T_m) of each sample determined by taking the first derivative of each sample and averaged across three replicates. **b)** Top panel: raw fluorescence intensity plotted against temperature for G12V-KRAS with or without NtAGO2 in the apo, GDP, or GTP-loaded state. Bottom panel: T_m of each sample determined by taking the first derivative of each sample and averaged across three replicates. The standard deviation of raw fluorescence between replicates is illustrated as a shaded area about the mean. **, $0.001 < P < 0.01$; ns, not significant.

SOS-mediated exchange, nor does it independently affect KRAS GTPase activity (Fig. S4), consistent with the low affinity of NtAGO2 for KRAS in the *in vitro* setting. Such would not allow it to compete with SOS, which binds nucleotide-free KRAS with low nanomolar affinity [28].

3. Discussion

The original goal of this study was to confirm a direct interaction and co-crystallize a complex between KRAS and FL AGO2. However, our SEC experiments performed using purified FL AGO2 expressed in insect cells did not demonstrate formation of such a complex with G12V-KRAS (Fig. S2). One explanation could be the existence of a specific proteoform or a higher order complex of AGO2 in living human cells that exhibits higher affinity for KRAS that cannot be replicated under our current conditions. It was previously reported that the ability of AGO2 to unwind miRNA was reduced in mutant-KRAS isogenic cell lines [11]. This suggests that KRAS may bind to a precursor form of AGO2 that is bound to an unprocessed miRNA duplex–a state difficult to trap *in vitro*. In more recent work, EGFR-mediated phosphorylation of AGO2 at Tyr393 was shown to prevent AGO2–KRAS association in cells. Because our FL AGO2 was expressed in a eukaryotic insect system, it is likely post-translationally modified differently than in cancer cells. Many different post-translational modifications have been reported for AGO2 including phosphorylation (at seven separate sites), PARylation, acetylation, ubiquitination, and hydroxylation [14]. These modifications are

context dependent as well. For instance, AGO2 was shown to be phosphorylated at Tyr393 by EGFR in response to hypoxic stress [29], a common state in solid tumors. The cellular milieu is also much different in a transformed cell, which likely changes how AGO2 is modified compared to a normal cell. Such may have also affected our results.

To avoid challenges imposed by miRNA loading and post-translational modification, we then pursued analysis of KRAS with a small fragment of AGO2 expressed in *E. coli*. We demonstrated that the purified FL and N-terminal domain of AGO2 can interact with KRAS independent of its nucleotide or mutational status. This is contrary to our general understanding of how KRAS interacts with its downstream effectors [3,28,30,31]. Although there are no other reported RAS effectors that recognize both conformations of KRAS, such an interaction is not impossible. For instance, a recently developed inhibitor, 2C07, binds to both the GTP-active and GDP-inactive conformations of RAS by inducing a novel switch II pocket [32], and the heterotrimeric G protein α has been reported to bind its effector adenylyl cyclase in both GDP and GTP-bound states, although with very different affinities [33]. It is also possible that antibody mediated methods of detection are overly sensitive, making it difficult to discern a difference in binding. Interestingly, our DSF measurements showed that addition of NtAGO2 reduced the apparent stability of KRAS regardless of its nucleotide state (Fig. 4). Though unable to assess in a quantitative manner due to the lack of a discrete melting temperature, NtAGO2 tended to have less of a destabilizing effect on apo KRAS than either nucleotide bound form. Less
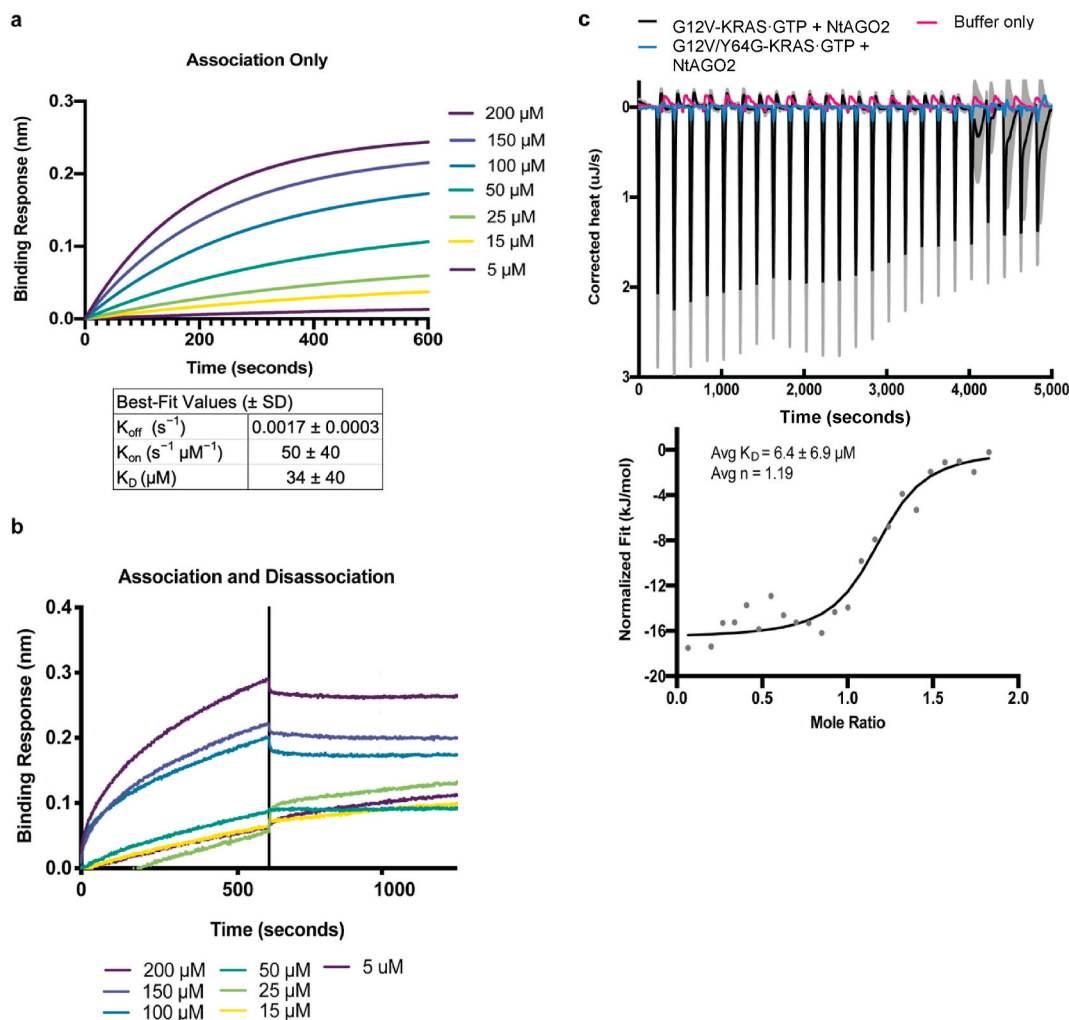
Fig. 5. Biochemical characterization of the KRAS–NtAGO2 interaction reveals non-equilibrium dependent disassociation. **a)** BLI of G12V-KRAS·GTP with increasing concentrations of NtAGO2. Table displays the calculated K_{off}, K_{on}, and K_D ± standard deviation following a non-linear regression of association data from multiple concentrations. Analysis was completed on the average of three triplicate experiments. **b)** Raw association and dissociation data of G12V-KRAS·GTP with increasing concentrations of NtAGO2. Dissociation was initiated following a 600 s association time and is marked by a black vertical line. One representative run is illustrated. **c)** Top right panel: ITC of G12V-KRAS·GTP (black) and G12V/Y64G-KRAS·GTP (blue) with NtAGO2. Buffer only control is shown in pink. The standard deviation of the heat released between two G12V-KRAS·GTP + NtAGO2 replicates is shown as a shaded grey area for each injection. Bottom right panel: independent fit of G12V-KRAS·GTP + NtAGO2 without assuming stoichiometry. Average K_D ± standard deviation and average mole ratio were calculated and are displayed at the top left corner of the bottom right panel. (For interpretation of the references to color in this figure legend, the reader is referred to the Web version of this article.)

destabilization was observed with G12V KRAS, suggesting that AGO2 has less of an effect on mutant KRAS's structural integrity. Together these data suggest that the binding between AGO2 and KRAS leads to conformational changes that destabilize at least some elements in the G protein. Based on this observation, we speculate that the N-terminal domain of AGO2 could, like GEFs [28], have preference for the nucleotide-free form of KRAS, which would be less accessible in the G12V mutant.

To attempt a quantitative assessment of the affinity of the interaction we used BLI and ITC. BLI measures the association and disassociation of an analyte (NtAGO2) to an immobilized bait protein (G12V-KRAS·GTP). In this technique we saw a concentration dependent association but incomplete disassociation, which, if taken at face value, would be similar to high affinity interactions (femto- and picomolar) such as those exhibited by antibody-antigen complexes. However, this interpretation is inconsistent with our SEC-MALS data which indicates low binding affinity (Figs. 2 and 5a, b). Analysis by a different technique, ITC also showed non-ideal behavior in that we observed an initial heat release, but the heat never fully returned to baseline (Fig. 5c). Although such binding data are not ideal, the interaction does seem specific as the

binding-deficient mutant G12V/Y64G-KRAS·GTP had no heat release upon titration into NtAGO2. The estimated K_D from both techniques was in the 6–35 μM range, consistent with our SEC results. Also consistent with our SEC, MALS, and IM-MS experiments, ITC calculated an approximate stoichiometry of 1:1. Furthermore, heat was released following the titration of G12V-KRAS into the sample cell containing NtAGO2, generating a net negative enthalpy of binding. This suggests the interaction is exothermic and likely driven by some combination of hydrogen bond networks, van der Waals forces, and/or salt-bridges.

From cellular and *in vivo* data [11,16], AGO2 inhibits KRAS signaling by preventing SOS-mediated nucleotide exchange. Thus, loss of AGO2 initiates oncogene-induced senescence by permitting excessive signaling through the WT RAS-axis. Crystal structures of SOS-bound RAS reveal that SOS extensively coordinates switch II, a region of RAS that is disordered in the apo or GDP-bound forms [28,34]. It is possible that, similar to SOS, AGO2 binding also results in ordering of switch II and stabilization of the apo-form of KRAS. However, consistent with previous work, we did not see a nucleotide preference when using purified components [11]. Using an *in vitro* GTPase assay, NtAGO2 has no effect on the ability of KRAS to either independently cycle nucleotide or

associate with SOS. It is possible that the fragment itself is too small to interfere in the same way that the full-length protein does, or that its binding is relatively weak compared to SOS.

The transient, low-affinity interaction we observed between both purified KRAS constructs and the purified N-terminal fragment of AGO2 (Figs. 1–3) is not entirely surprising. Many proteins in signal transduction pathways bind to their partners with relatively low affinity and transient complexes are an important adaptation allowing for a quick and dynamic response to changes in extracellular stimuli[35,36]. The low affinity could also be due to the instability and poor behavior of the fragment itself. Normally, in the full-length structure, the N domain of AGO2 is shielded by the second linker region and the complexed small RNA. It is possible that these regions are now solvent exposed causing the fragment to precipitate and/or aggregate, making quantitative measurements difficult. Although the data presented in this study do confirm a direct association of KRAS with the RNAi machinery, crystallization of KRAS with an NtAGO2 fragment is improbable and future studies are necessary to determine and enrich the proteo-form of FL AGO2 that is most compatible with KRAS binding to enable structural analysis.

4. Methods

Construct Generation: Human KRAS4b constructs included just the core G-domain which spans from amino acids 1–166 and excluded the C-terminal hypervariable region. QuikChange II (Agilent, #200521) site directed mutagenesis was used to generate the G12V and Y64G/G12V variants. Constructs were sequenced via Sanger sequencing to ensure mutations were present and in the correct position. Because an initial N-terminal fragment of human AGO2 spanning residues 50–141 could not be purified due to insolubility, the NtAGO2 construct used in these studies spanned residues 55–137. The termini were chosen based in part on the crystal structure of the FL AGO2 protein (PDB entry 4W5N) [37] and to minimize the presence of hydrophobic residues in unstructured regions. These KRAS and AGO2 variants were cloned into pET21 vectors containing a 6x-Histidine tag followed by a tobacco etch virus protease cleavage site. The pFB GFP HFT-AGO2 3xD2xA plasmid and P1 virus encoding full length human AGO2 was provided by Ian MacRae (Scripps Research Institute) and contained 5 mutations (T357D, S824A, S828D, S831D, S833A) that increase protein expression in baculovirus infected insect cells [12]. These mutations are of surface residues that are known sites of phosphorylation that are distant from the expected KRAS binding site.

Protein Expression and Purification: KRAS and NtAGO2 variants were expressed in *E. coli* Rosetta (DE3) pLysS cells (Novagen). In each case, 8 L of cells were grown in Terrific Broth (EMD Millipore Sigma) supplemented with 2.5% glycerol and 1 mM ampicillin at 37 °C until an A_{600} of ~1.0 was reached. The temperature was lowered to 18 °C and KRAS expression was induced with 1 mM isopropyl-β-d-1-thiogalactopyranoside. The cells were grown for an additional 18 h, harvested and pelleted at 5000 rpm for 30 min. Cell pellets were resuspended in either 25 mM HEPES pH 7.5, 200 mM NaCl, 0.5 mM dithiothreitol (DTT) for G12V-KRAS, or 50 mM Tris pH 8.0, 300 mM NaCl, 0.5 mM DTT for NtAGO2 containing 1 μM leupeptin and 0.1 μM phenylmethylsulfonyl fluoride (PMSF). Deoxyribonuclease I (DNase I) or benzonase was added to remove excess nucleic acid. Cells were sonicated and soluble portions were collected following centrifugation at 15,000 rpm for 45 min. KRAS and NtAGO2 proteins were purified via Ni^{2+} affinity resin (Thermo-Fisher Scientific, catalog #88222) in a gravity column. The His-tag was removed overnight in dialysis using 5% (w/w) of purified TEV protease and the protein was further purified by passage through an additional Ni^{2+} column. The KRAS constructs were then concentrated and dialyzed in nucleotide exchange buffer containing 10 mM EDTA. Exchanged protein was reconstituted with either GDP, GTP, or GMP-PNP (Sigma-Aldrich, G0635-25 MG) at 10x molar excess and the loading reaction was quenched with 10 mM $MgCl_2$. The protein then underwent a final

purification step via SEC using a 10/300 analytical Superdex 75 column (GE Healthcare) to remove excess nucleotide and exchange into reaction buffer containing 25 mM HEPES pH 7.5, 200 mM NaCl, 0.5 mM DTT and 10 mM $MgCl_2$. After the second Ni^{2+} column, NtAGO2 was concentrated and processed immediately by 10/300 analytical S75 column. Protein purity was >98% as assessed by SDS-PAGE. Full length AGO2 was expressed and purified via methods previously described [12].

Immunoprecipitation (IP) and Western Blot Analysis. For IP analysis, K-buffer (20 mM Tris pH 7.0, 150 mM NaCl, 1% Triton X100, 1 mM DTT, and 1 μM leupeptin) was added to a final volume of 500 μl of samples containing 100 ng of each purified protein. These samples were pre-cleared with 10 μl of Dynabeads (Invitrogen) for 1 h. Pre-cleared samples were incubated with 10 μg of the RAS10 primary antibody (Millipore, 05–516), at 4 °C overnight. 30 μl of equilibrated Dynabeads were then added to immune complexes and incubated for 2–3 h at 4 °C, centrifuged, and washed in K-buffer prior to separation of immunoprecipitates by SDS-PAGE. The sample control IPs were performed using a normal mouse IgG primary antibody (Sigma-Aldrich, 12–371). Samples were separated on a 15 well gradient gel, transferred onto nitrocellulose membrane using a BioRad wet transfer system, and blocked with 2.5% BSA in TBS-Tween (0.1%). The RAS10 primary antibody (Millipore, 05–516), and AGO2 primary antibody (AGO2 (SinoBiological, 50683-RO36) were incubated at 1:1000 ratio overnight at 4 °C. Blots were washed in TBS-Tween (0.1%) and incubated with Licor compatible secondary antibodies and imaged using a Licor imager.

Image Acquisition, Equipment, and Settings. A Licor imager was used to image western blots. Images were collected using two separate channels, one for each primary antibody. A red channel was used for detecting signal from the RAS10 primary and Licor compatible mouse secondary antibody and the green channel was used for detecting signal from the AGO2 primary and Licor compatible rabbit secondary antibody. No image editing was done on other software.

Lumit ImmunoAssay. Purified SUMO protease was acquired from the Center for Structural Biology (University of Michigan). Purified catalytic domain of SOS1 was purchased from Cytoskeleton (product # CS-GE02). RAS10 (Millipore, 05–516), AGO2 (SinoBiological, 50683-RO36), SOS (Abcam, ab140621), and SUMO (BioVision, A1455-100) primary antibodies were used at the indicated ratios. Secondary antibodies were included in the Lumit ImmunoAssay kit *(Promega, W1201)* and experiments performed as per the manufacturer instructions. Luminescence values were determined by fold change from sample containing RAS10 primary antibody and were analyzed using GraphPad Prism 7. Experiments were performed 4 times in triplicate using two separate protein preparations. Students T-test was used to determine significance and a p-value of 0.05 was used as a cut-off for significance.

Complex Formation, SEC, and MALS: Purified recombinant proteins were incubated together at a 2:1, NtAGO2:RAS, molar ratio for 15 min on ice and the protein complex was separated from individual components using either an S75 10/300 (GE Healthcare) column for isolated SEC experiments, or a Protein KW-804 column (Shodex) coupled to a Dawn-Helios MALS detector to determine the absolute molecular weight and stoichiometry of the complex. Both NtAGO2 and KRAS proteins were also analyzed independently as controls. Data points were plotted using GraphPad Prism 7.

Ion-Mobility Mass Spectrometry (IM-MS): Individual proteins were expressed and purified as described above except Tris-HCL pH 8.0 was used in place of HEPES buffer. The final sample buffer included only 25 mM Tris pH 8.0 and 150 mM NaCl to enable more efficient buffer exchange into IM-MS buffer. G12V-KRAS was loaded with 10x molar excess GMPPNP via methods describe in the above section and excess nucleotide was removed from the sample using in a final S75 10/300 polishing step. Samples were prepared by mixing 20 μM of purified NtAGO2 with 10 μM G12V-KRAS. These were kept on ice and immediately prepared for data collection. Prior to analysis, the samples were buffer exchanged into 200 mM (pH~7) ammonium acetate using Bio-Rad Bio-Spin 6 columns. Samples were transferred to the gas phase by

nanoelectrospray ionization (nESI) using gold-coated borosilicate capillaries. All measurements were conducted on a modified Agilent 6560 drift tube ion mobility mass spectrometer optimized for native protein measurements [24]. IM measurements were conducted in high purity nitrogen (N_2), at five different electric field strengths (15.96, 16.61, 17.25, 17.89, 18.53 V/cm), enabling collision cross section ($^{DT}CCS_{N_2}$) measurement by the stepped-field method [38]. All $^{DT}CCS_{N_2}$ measurements were converted to helium measurements ($^{DT}CCS_{He}$) using a previously established relationship [39], to enable comparison of our experimental ^{DT}CCS values with theoretical CCS values ($^{T}CCS_{He}$) generated for computationally docked structures. The $^{DT}CCS_{N_2}$ and the calculated $^{DT}CCS_{He}$ values are reported in Table S1. $^{T}CCS_{He}$ values computed for all docked structures are reported in Table S2. Raw data was analyzed using Agilent IM-MS Browser 10.0. Extraction, and Gaussian fitting of IM arrival time distributions was carried out using CIUSuite2 [40]. The $^{T}CCS_{He}$ values for the docked KRAS–NtAGO2 structures were computed using IMPACT projection approximation [26]. The signal intensities (I) from the 2D plots were used to quantify the fraction of complex using the following relationship:

$$\frac{I_{KRas-NtAgo(11+,\,10+)}}{I_{Kras-NtAgo(11+,\,10+)} + I_{NtAgo\,(7+,\,6+,\,5+)} + I_{KRas\,(9+,8+,7+)}}$$

Simulated KRAS–NtAGO2 Docking: Two individual docking experiments were performed using pyDockWEB [25]. PDB files for G12V KRAS-GDP (PDB: 4TQ9) and WT KRAS·GMPPNP (PDB: 6GOD) were analyzed using the PyMOL Molecular Graphics System to ensure only one chain was represented. PDB 4W5N of full length AGO2 was trimmed to residues 55–137 and saved as a new PDB file representing the NtAGO2 fragment. Each experiment generated 100 predicted complex structures. Theoretical CCS values were computed using IMPACT projection approximation.

Differential Scanning Fluorometry (DSF): Protein thermal stability was assessed with an HT7900 qPCR instrument using 0.25 mg mL^{-1} G12V-KRAS, KRAS, NtAGO2, or RAS–NtAGO2 complex in assay buffer (25 mM HEPES pH 7.5, 200 mM NaCl, 0.5 mM DTT) containing SYPRO Orange protein gel stain (500x stock, Sigma-Aldrich) and a variety of additives including 5 μM GTP, 5 μM GDP, and 1 mM MgCl$_2$, as indicated. Melt curves were obtained by increasing the temperature from 25 to 70 °C at a rate of 2 °C min^{-1}. Data were plotted in GraphPad Prism 7 where the peak of the 1st derivative of each curve represents the melting point (T_m) of the protein. Experiments were performed 3x each in triplicate from two independent protein preparations.

Biolayer Interferometry (BLI): G12V-KRAS·GMPPNP was biotinylated using EZ-Link™ NHS-PEG4-Biotin No-Weigh™ Format (Thermo Scientific # PIA39259). The protein was passaged over an S75 10/300 SEC column to separate it from excess biotin. The biotinylated protein was then loaded onto streptavidin sensors, washed, and dipped into varying concentrations of NtAGO2. Binding response was plotted vs. time and GraphPad Prism 7 was used to determine association kinetics from 5 different concentrations of ligand. In order to calculate the equilibrium binding constant, K_D where $K_d = k_{off}/k_{on}$, the k_{obs} from association only were determined at each concentration and plotted against NtAGO2 concentration. The slope of the line corresponded to k_{on} while the y-intercept is k_{off} using the equation $k_{obs} = k_{on}[NtAGO2] + k_{off}$.

Isothermal Titration Calorimetry: Using a TA NanoITC instrument, pre-dialyzed G12V- or G12V/Y64G-KRAS (0.6 mM) was injected 25x into the sample cell containing N-terminal AGO2 fragment (0.1 mM) that was dialyzed together with the RAS construct being measured. Injection enthalpy (kJ/mol) was plotted verses the mole ratio. Binding affinity, stoichiometry, enthalpy and entropy for the integration were calculated and curves were fit using NanoITC Analyze software without assuming stoichiometry. Because the heat release did not return to baseline, we did additional experiments where either dialysis buffer alone or dialysis buffer containing excess nucleotide was titrated into a sample cell containing dialysis buffer to ensure that the buffers were not mismatched and that the heat measured was not due to dissociated nucleotide.

4.1. In vitro assay to measure KRAS·GTP levels

KRAS variants were expressed and purified via the procedure outlined above. Freshly purified protein was assayed to determine the appropriate protein concentration to optimizing intrinsic GTPase activity. Purified catalytic domain of SOS1 (Cytoskeleton) was used to carry out nucleotide exchange. Purified components were added as indicated, and KRAS-GTP levels were estimated using the GTPase-GLO assay from Promega (product #V7681), following the manufacturer instructions.

4.2. Statistical analyses

GraphPad prism was used for all statical analysis. T-tests were used to compare the means of desired groups. A p-value of 0.05 was used as the significance cut off.

Author contributions

Protein expression and purification was done by J.J.W. IP-Western, Lumit Immunoassay, SEC, MALS, ITC, BLI, and GTPase assays, data analysis, data presentation, and manuscript preparation were done by J.J.W. Sample preparation for IM-MS experiments was done by J.J.W, data acquisition, analysis, and data presentation were done by V. V.G. and B.T.R. T.S.B and J.J.G.T aided in experimental design, data collection, and data analysis. C.K. aided in sample preparation and IP-Western experiments. R.F.S, S·S, and all other authors assisted in manuscript editing. Supervision and funding of this study were provided by J.J.G.T and A.M.C.

Declaration of competing interest

The authors declare that they have no known competing financial interests or personal relationships that could have appeared to influence the work reported in this paper.

Data availability

Data will be made available on request.

Appendix A. Supplementary data

Supplementary data to this article can be found online at https://doi.org/10.1016/j.bbrep.2021.101191.

References

[1] A.D. Cox, C.J. Der, Ras history, Small GTPases 1 (2014) 2–27.

[2] Y. Pylayeva-Gupta, E. Grabocka, D. Bar-Sagi, RAS oncogenes: Weaving a tumorigenic web, Nat. Rev. Cancer 11 (2011) 761–774.

[3] M.V. Milburn, et al., Molecular switch for signal transduction: structural differences between active and inactive forms of protooncogenic ras proteins, Science 247 (1990) 939–945.

[4] E.F. Pai, et al., Refined crystal structure of the triphosphate conformation of H-ras p21 at 1.35 A resolution: implications for the mechanism of GTP hydrolysis, EMBO J. 9 (1990) 2351–2359.

[5] R. Gasper, F. Wittinghofer, The Ras switch in structural and historical perspective, Biol. Chem. 401 (2019) 143–163.

[6] S.R. Sprang, How Ras works: structure of a Rap-Raf complex, Structure 3 (1995) 641–643.

[7] T. Travers, et al., Molecular recognition of RAS/RAF complex at the membrane: role of RAF cysteine-rich domain, Sci. Rep. 8 (2018), 8461–15.

[8] A.D. Cox, S.W. Fesik, A.C. Kimmelman, J. Luo, C.J. Der, Drugging the undruggable RAS: mission possible? Nat. Rev. Drug Discov. 13 (2014) 828–851.

[9] D.K. Simanshu, D.V. Nissley, F. McCormick, RAS proteins and their regulators in human disease, Cell 170 (2017) 17–33.

[10] A.N. Hata, A.T. Shaw, Resistance looms for KRASG12C inhibitors, Nat. Med. 26 (2020) 169–170.

[11] S. Shankar, et al., KRAS engages AGO2 to enhance cellular transformation, Cell Rep. 14 (2016) 1448–1461.

[12] N.T. Schirle, I.J. MacRae, The crystal structure of human Argonaute2, Science 336 (2012) 1037–1040.

[13] J. Liu, et al., Argonaute2 is the catalytic engine of mammalian RNAi, Science 305 (2004) 1437–1441.

[14] D. Jee, E.C. Lai, Alteration of miRNA activity via context-specific modifications of Argonaute proteins, Trends Cell Biol. 24 (2014) 546–553.

[15] J.-T. Huang, J. Wang, V. Srivastava, S. Sen, S.-M. Liu, MicroRNA machinery genes as novel biomarkers for cancer, Front. Oncol. 4 (2014) 113.

[16] S. Shankar, et al., An essential role for Argonaute 2 in EGFR-KRAS signaling in pancreatic cancer development, Nat. Commun. 11 (2020), 2817–17.

[17] P.B. Kwak, Y. Tomari, The N domain of Argonaute drives duplex unwinding during RISC assembly, Nat. Struct. Mol. Biol. 19 (2012) 145–151.

[18] P. Chardin, et al., Human Sos1: a guanine nucleotide exchange factor for Ras that binds to GRB2, Science 260 (1993) 1338–1343.

[19] V.V. Gadkari, et al., Investigation of sliding DNA clamp dynamics by single-molecule fluorescence, mass spectrometry and structure-based modeling, Nucleic Acids Res. 46 (2018) 3103–3118.

[20] I.S. Camacho, et al., Native mass spectrometry reveals the conformational diversity of the UVR8 photoreceptor, Proc. Natl. Acad. Sci. U. S. A. 116 (2019) 1116–1125.

[21] B.A. Meinen, V.V. Gadkari, F. Stull, B.T. Ruotolo, J.C.A. Bardwell, SERF engages in a fuzzy complex that accelerates primary nucleation of amyloid proteins, Proc. Natl. Acad. Sci. U. S. A. 116 (2019) 23040–23049.

[22] J.W. Wilson, A.D. Rolland, G.M. Klausen, J.S. Prell, Ion mobility-mass spectrometry reveals that α-hemolysin from Staphylococcus aureus simultaneously forms hexameric and heptameric complexes in detergent micelle solutions, Anal. Chem. 91 (2019) 10204–10211.

[23] S.K. Thangaraj, et al., Quantitation of thyroid hormone binding to anti-thyroxine antibody fab fragment by native mass spectrometry, ACS Omega 4 (2019) 18718–18724.

[24] V.V. Gadkari, et al., Enhanced collision induced unfolding and electron capture dissociation of native-like protein ions, Anal. Chem. 92 (2020) 15489–15496.

[25] B. Jiménez-García, C. Pons, J. Fernández-Recio, pyDockWEB: a web server for rigid-body protein-protein docking using electrostatics and desolvation scoring, Bioinformatics 29 (2013) 1698–1699.

[26] E.G. Marklund, M.T. Degiacomi, C.V. Robinson, A.J. Baldwin, J.L.P. Benesch, Collision cross sections for structural proteomics, Structure 23 (2015) 791–799.

[27] J.L.P. Benesch, B.T. Ruotolo, Mass spectrometry: come of age for structural and dynamical biology, Curr. Opin. Struct. Biol. 21 (2011) 641–649.

[28] P.A. Boriack-Sjodin, S.M. Margarit, D. Bar-Sagi, J. Kuriyan, The structural basis of the activation of Ras by Sos, Nature 394 (1998) 337–343.

[29] J. Shen, et al., EGFR modulates microRNA maturation in response to hypoxia through phosphorylation of AGO2, Nature 497 (2013) 383–387.

[30] I.R. Vetter, A. Wittinghofer, The guanine nucleotide-binding switch in three dimensions, Science 294 (2001) 1299–1304.

[31] K. Scheffzek, et al., The Ras-RasGAP complex: structural basis for GTPase activation and its loss in oncogenic Ras mutants, Science 277 (1997) 333–338.

[32] D.R. Gentile, et al., Ras binder induces a modified switch-II pocket in GTP and GDP states, Cell Chem Biol 24 (2017), 1455–1466.e14.

[33] R.K. Sunahara, C.W. Dessauer, R.E. Whisnant, C. Kleuss, A.G. Gilman, Interaction of Gsalpha with the cytosolic domains of mammalian adenylyl cyclase, J. Biol. Chem. 272 (1997) 22265–22271.

[34] J. Cherfils, Ras Superfamily Small G Proteins: Biology and Mechanisms, vol. 1, Springer Vienna, 2014, pp. 51–63, https://doi.org/10.1007/978-3-7091-1806-1_3.

[35] S.E. Acuner Ozbabacan, H.B. Engin, A. Gursoy, O. Keskin, Transient protein-protein interactions, Protein Eng. Des. Sel. 24 (2011) 635–648.

[36] D. Szklarczyk, et al., STRING v11: protein-protein association networks with increased coverage, supporting functional discovery in genome-wide experimental datasets, Nucleic Acids Res. 47 (2019) D607–D613.

[37] N.T. Schirle, I.J. MacRae, The crystal structure of human Argonaute2, Science 336 (2012) 1037–1040.

[38] E.W. McDaniel, E.A. Mason, Transport properties of ions in gases. Liver Metastasis: Biology and Clinical Management, Springer, Dordrecht, 1988, https://doi.org/10.1002/3527602852.

[39] R.T. Kurulugama, E. Darland, F. Kuhlmann, G. Stafford, J. Fjeldsted, Evaluation of drift gas selection in complex sample analyses using a high performance drift tube ion mobility-QTOF mass spectrometer, Analyst 140 (2015) 6834–6844.

[40] D.A. Polasky, S.M. Dixit, S.M. Fantin, B.T. Ruotolo, CIUSuite 2: next-generation software for the analysis of gas-phase protein unfolding data, Anal. Chem. 91 (2019) 3147–3155.